Differential Photometry of
Active Galactic Nuclei using
Time Resolved Observations with the
1m Nickel Telescope of Lick Observatory

Chance Lucas Spencer

California Polytechnic University - San Luis Obispo
A thesis submitted in partial fulfillment
for the degree of Bachelor of Science in Physics
Summer 2019

Advisor:
Dr. Vardha N. Bennert

Contents

1 Abstract

Active galactic nuclei (AGNs) are exotic objects in the center of some galaxies with luminosities that can greatly outshine the stars of the host galaxy across the entire electromagnetic spectrum. The origin of the UV/optical light is thought to be due to accretion of material onto the supermassive black hole in their centers. Since these objects are too far away to resolve the gravitational sphere of influence of the black hole directly, we make use of a method called reverberation mapping. We measure the lag between the AGN power-law continuum emitted by the accretion disk and the Doppler-broadened emission lines which originate in gas clouds orbiting the black hole at high speeds while being ionized by the power-law continuum. Using light travel time arguments, the observed lag time can be translated into the size of the broad-line region. Combined with the width of the broad emission lines, we can estimate the black hole mass.

The Seoul AGN Monitoring Project (SAMP) uses the 1m Nickel telescope of Lick Observatory to study the variability of the optical continuum emission. Combining these observations with spectroscopy of the broad-line region of the same AGNs, we can perform reverberation mapping. Our team, consisting of a handful of Cal Poly undergraduate students, is in charge of the optical imaging, controlling the 1m telescope remotely from Cal Poly. In this thesis, I present an overview of the optical imaging campaign led by the Cal Poly undergraduate students as well as first results of the observed continuum variability of the AGNs studied. Our study is special in that it targets AGNs at the high-mass end over a multi-year long campaign.

2 Introduction

2.1 Overview and History of AGNs

Active Galactic Nuclei (AGN) are objects that reside in the center of galaxies and exhibit energies 100 - 1000 times greater than the collective light of the host galaxies they occupy and cannot be simply explained by stellar mechanisms. Two of the largest and most researched sub-classes of AGNs are Seyfert galaxies and quasars. Seyfert galaxies have nuclear sources which emit a total energy at visible wavelengths on the order of 10^{11} L$\odot$ while a quasar has a nuclear source which is brighter than that by a factor of 100 or more. The fundamental properties of AGNs are that they are star-like objects that have a continuum flux that is time-variable, a large ultra-violet (UV) flux, broad emission lines, and a large redshift. The most common of all these properties associated with AGNs is a luminous X-ray source. Unless stated otherwise, the material in the following sections is referenced from *An Introduction to Active Galactic Nuclei*. [5]

In 1908, Lick Observatory was the first place to ever receive an optical spectrum from an AGN. Carl Seyfert attempted to categorize a large group of galaxies and noted that the galaxies with high-excitation nuclear emission lines had broad lines as well as hydrogen lines that were sometimes broader than the other lines. It was also found that the nuclei were unresolved which meant the nucleus must be less than 100 pc, the change in variability of nuclear emissions must last a long time, and the mass of the nucleus must be very large.

2.2 AGN Components

2.2.1 Accretion Disk

The main driver of the energetic properties we see from AGNs is the accretion disk where the accretion of matter onto a disk around the black hole takes place. The energy is generated from viscous friction forces from the matter of the material around the black hole. By assuming the source is stable and isotropic, meaning the force of radiation pressure outward has to be equally counteracted by the force of gravity inward, the Eddington limit gives a minimum mass for a certain luminosity. The Eddington luminosity gives the maximum luminosity of a source of mass M assuming the luminosity is from accretion. By finding the mass through the virial theorem (M $\approx \text{v}^2/\text{G}$) and using the velocity of the matter in the broad line region by the Doppler broadening it exhibits, the estimate of the mass is an order of magnitude larger than the Eddington mass. The Eddington mass only requires 1-2 solar masses that are accreted every year to output the observed luminosities. The following equation is a version of Einstein's famous mass-to-energy equation with an efficiency factor included:

$$E = \eta mc^2 \tag{1}$$

In certain oversimplified conditions, $\eta \approx 0.1$ for matter falling within 5 Schwarzschild radii of an 8 solar mass black hole, which is more efficient than fusion of hydrogen to helium which has a $\eta \approx 0.007$. The main problem to this type of energy source is when angular momentum is considered. While travelling inward to an accretion disk, infalling gas must lose a majority of its angular momentum. This is one reason to suspect interactions with other galaxies contribute to fueling AGNs since they will remove a lot of angular momentum. The gas required for accretion

may be generated and taken from stars if they are close enough to be tidally disrupted by their black holes. Stars may also lose some of their mass via stellar winds depending on their evolutionary stage. Gas from the stars is lost but angular momentum is conserved, so the gas forms an accretion disk.

With regards to the accretion disk, the gravitational energy is half converted into heating the gas and the other half is radiated away by the heated gas as blackbody radiation. The radius of the nucleus seems to be within the range of 1 pc < r < 100 pc. The mass of the nucleus is found on a range of $M^{9\pm1}$ M_{Sun}. For a 10^8 M_{Sun} black hole, the inner accretion disk emits a frequency of 3.6 x 10^{16} Hz, which is in the extreme UV and soft X-ray region.
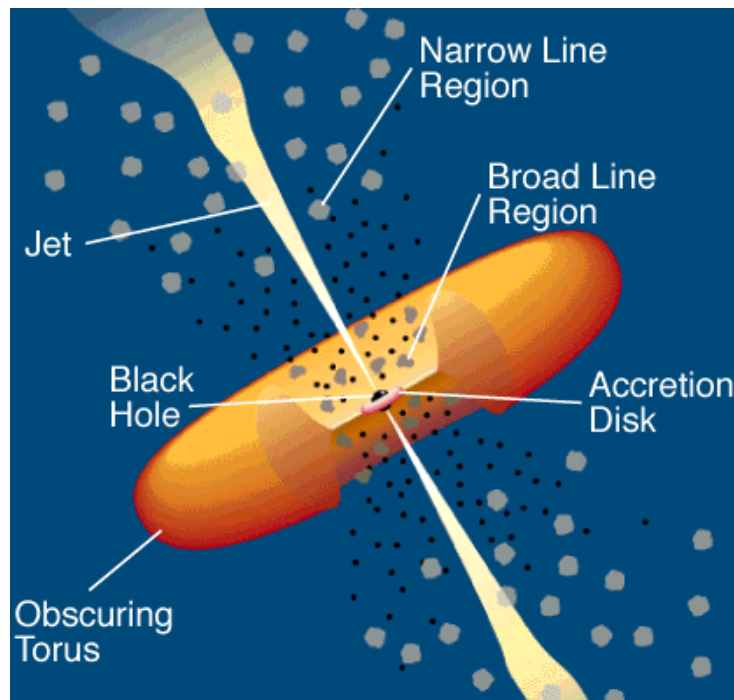

Figure 1: A universally accepted model of the different regions in an AGN.
(Urry & Padovani, 1995)

2.2.2 The Broad Line Region

The broad line region (BLR), typically having a radius < 0.1 pc, provides a lot of useful information on AGNs since its bulk motion is caused by the gravity of the central source. The orbital velocities in this region range from 500 km s^{-1} to 5000 km s^{-1}. Broad lines in broad-line regions are assumed to be Doppler-broadened and are given in units of velocity (km s^{-1}). This is done either at full width half max (FWHM) intensity or full width zero intensity (FWZI), the latter being more uncertain due to the possibility of other lines combining. This line blending is due to large Doppler broadening. Since line structures vary so much, it is assumed that the line strengths are a function of line-of-sight velocity. It seems that the accretion disk is ionizing the gas in the BLR since the emission lines have fluxes that correlate with the continuum fluxes. It is also predicted that a majority of recombination emissions comes from optically thick clouds in the ionizing continuum. Another feature of the BLR is that there are no forbidden lines that

are broad, implying that the BLR is dense. Forbidden lines are emission lines that are typically prevented from a quantum-mechanical selection rule and are "collisionally suppressed." This is because in a dense region, it is more likely that an excited electron will be collisionally de-excited rather than transitioning (which would need a longer time to wait for it to occur).

As stated previously, since the variation in the emission-line fluxes in the BLR match the continuum flux changes, it is assumed that photoionization due to UV radiation from the accretion disk is ionizing the BLR. Ionized hydrogen then re-emits light upon recombination, emitting Balmer lines that we are able to observe. Models depend on the ionizing continuum's shape, the chemical composition, and the particle density of the cloud.

2.2.3   The Narrow Line Region

The narrow line region (NLR) is a spatially extended region (100 pc - 1000 pc) outside of the broad line region, and its kinematic and physical distributions can be mapped out directly from the emissions. The gas in this region has orbital velocities that range from 200 km s^{-1} to 900 km s^{-1}, relatively slower than in the BLR. Forbidden transitions are not collisionally suppressed in the NLR since electron densities are low. The ratio between certain forbidden line pairs allows us to measure electron densities and temperatures of the gas in this region, which range from 10000 K to 25000 K. The only downside to analyzing this region is that there is dust present since the NLR is extended and outside the dust sublimation radius of the AGN.

In low electron density scenarios, the radiative process is so quick that almost all collisional excitations are followed by radiative de-excitation. In a high electron density scenario, de-excitation is more likely to occur collisionally instead of radiatively. Emission lines are also able to give an estimate of the electron temperature as well. The intensity ratio between a pair of two emission lines depends on electron density, and in other scenarios, on electron temperature.

By using the luminosity of specific strong lines, the radius as well as mass of the NLR can be estimated. It is also known that the NLR is clumpy as seen in high-resolution spectra since the region is at least partially resolvable. Short-term narrow-line variability is not expected since the region is at least 300 light-years wide.

Narrow-line emission profiles are usually blueward asymmetric and are non-Gaussian with bases that are wider than Gaussian. This is due to outflows which is gas flowing out and towards us (blueshifted) on the side closer to us. On the far side, the gas that is outflowing away from us (redshifted) is blocked by dust. It has also been noted that there is a relationship between the luminosity of the galactic bulge and the line width of [O$_{III}$] λ5007. NLR widths describe the gravitational field of the stars compared to the BLR line widths which follow the gravitational potential of the BH. It is possible that the NLR merges naturally with the BLR, if the density and velocity dispersion increase further in towards the center of the object.

NLRs are found to be axisymmetric instead of spherically symmetric, which means the NLR axis is the same as the radio axis in AGNs where radio emissions occur. "Ionizing cones" are wedge-shaped structures where the [O$_{III}$] λ5007/Hβ flux ratio is greater than outside the cone which indicates that the gas within the ionization cone is ionized by the AGN (while outside, it is either not ionized or ionized by stars). Ionization cones can be single-sided or bi-conical structures.

2.3   The Unified Model of AGNs

Regarding Seyfert galaxies, there are two types: Seyfert-1 and Seyfert-2. Below is an example of the emission spectra of a Seyfert-1 galaxy and Seyfert-2 galaxy for comparison. In the Seyfert-1 example on top, the broad lines are visible and the power-law continuum is visible. In the example below it, the Seyfert-2 example only has narrow lines and and no power-law continuum is visible, but instead absorption lines from the underlying stars of the host galaxy.
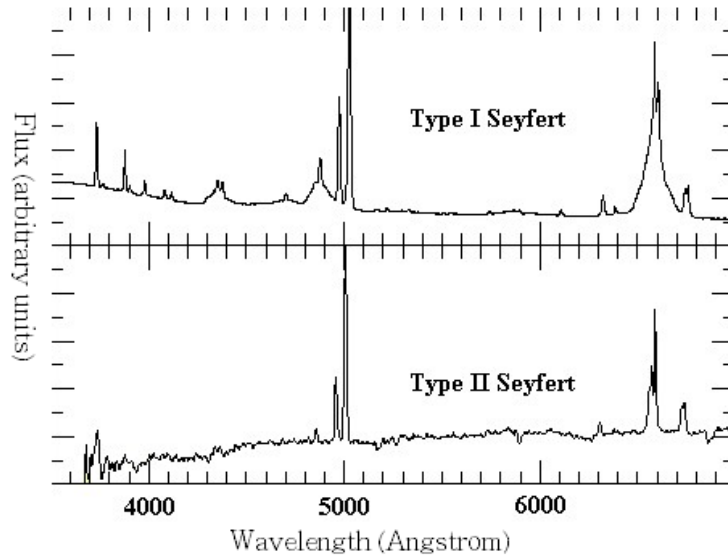

Figure 2: Emission lines of Seyfert-1 and Seyfert-2 galaxies. (Morgan 2002)

From unification studies, it has been suggested that type 1 and type 2 Seyfert galaxies are intrinsically the same, but that the viewing angle of a Seyfert galaxy from our perspective can affect what we see. The unification theory suggests that if AGNs have a dusty torus and we are observing a Seyfert galaxy "edge on", the broad lines from the BLR and the continuum emission from the accretion disk are absorbed by the dusty torus and only narrow lines are observed. From an observer's perspective, we would conclude we were observing a Seyfert-2 galaxy. If we were looking down axis of the torus at the plane of the accretion disk, broad lines would be unobstructed and we would state we were looking at a Seyfert-1 galaxy. Support for this model came from observing broad lines in polarized light from Seyfert-2 galaxies due to electrons scattering BLR emission into our line of sight. (Scattered light is polarized.)
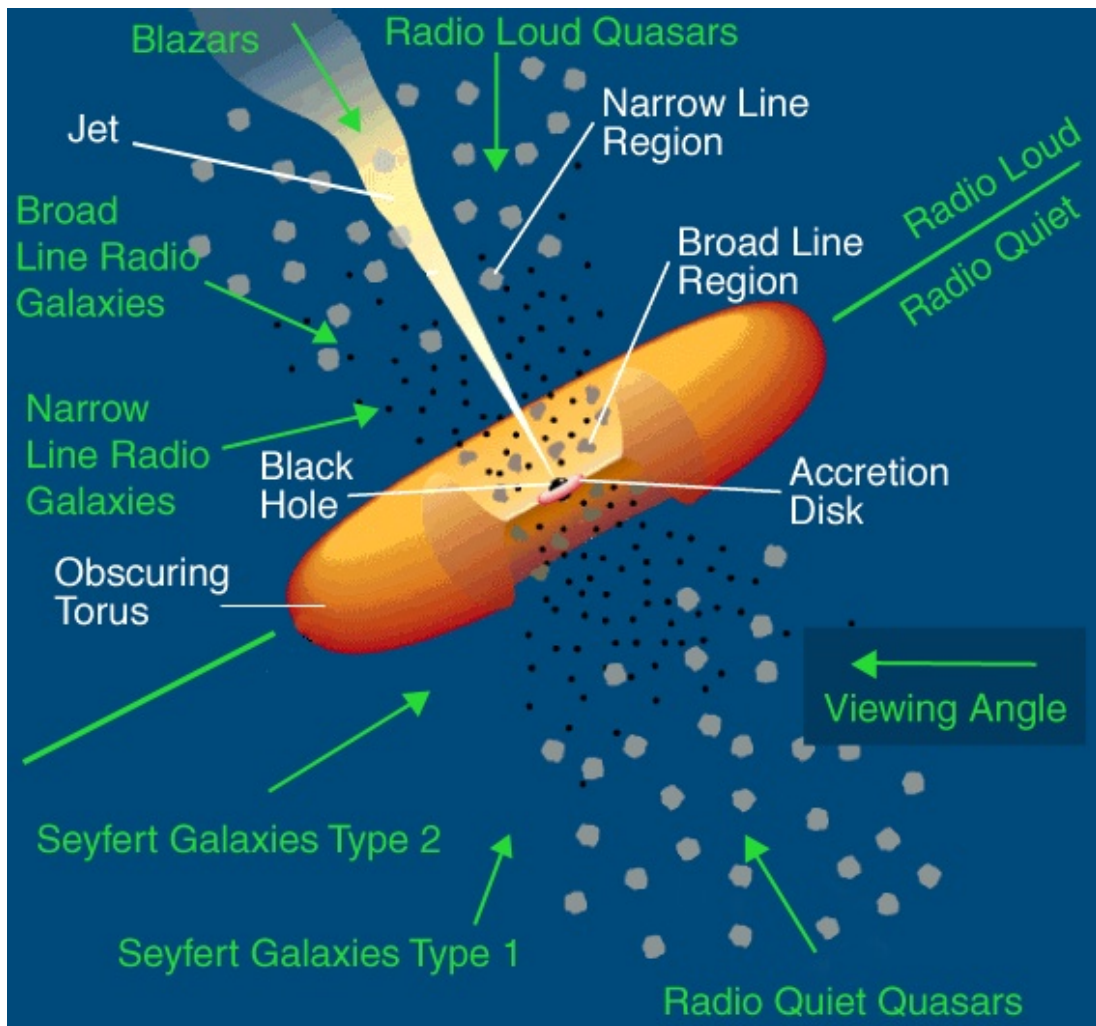
Figure 3: The viewing angle of the observer may affect whether a Seyfert-1 or Seyfert-2 is observed. (Modified figure from Urry & Padovani, 1995)

2.4 Reverberation Mapping

Using a technique called reverberation mapping, we are able to estimate the masses of the black holes in the center of AGNs by collecting three sets of data: the flux of the central source from photometry, the flux of the BLR via spectroscopy, and the velocity of the gas in the BLR using the Doppler broadening from spectra in that region. By comparing the delay between the continuum changes from the accretion disk and the emission lines changes in the BLR, we are able to calculate the radius of the BLR due to the light travel time between the central source and the broad line region. The larger black hole masses result in larger luminosities which can ionize the BLR to larger radii, resulting in longer time lags. The variation in BLR emission lines stems from continuum variations in the center of the AGN. In Figure 4, an example of an isodelay surface for an arbitrary time is shown that assumes that the BLR is a uniform spherical shell of radius r. The clouds responding at this particular time are shown by the intersection of the radial photon paths with the BLR surface.
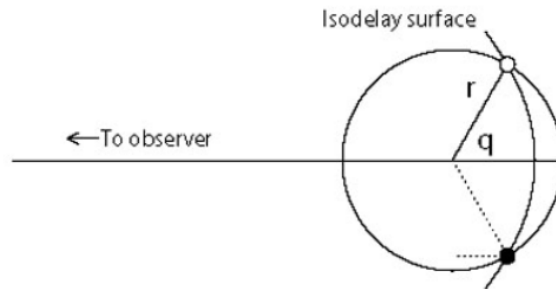
Figure 4: A model of an isodelay surface with respect to an observer. (Peterson et al., 1997)

With the data above, we can make a light-curve for these two regions which shows how their flux changed over a certain amount of time. The following graph is an example of what our light-curves would look like:
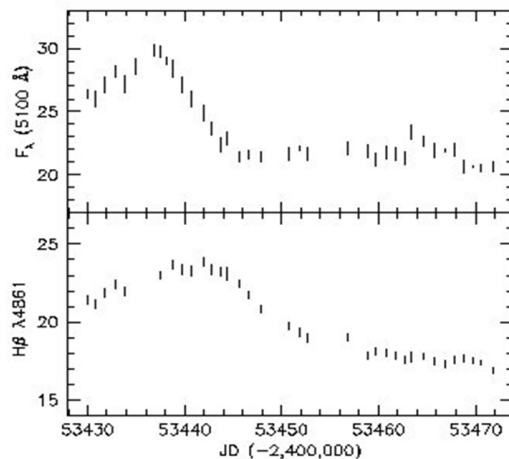
Figure 5: Variation in flux (arbitrary units) of both the accretion disk, as traced by the continuum emission at 5100 Angstrom (top panel) and as traced by the broad Hβ line (bottom panel) in light-days. (Bentz et al. 2006)

The number of days between two peaks in flux can be converted to a distance in light days (the distance light traveling at the speed of light would travel in those days). This gives us a radius for the BLR. By using the following relation, we are able to estimate the masses of the central black hole:

$$M_{BH} \propto \frac{R_{BLR} \times v_{BLR}^2}{G} \tag{2}$$

The proportionality stems from us not knowing either geometry or kinematics of the BLR. One motive for our project is finding a more accurate proportionality factor to make our equation a better predictor of black hole masses, especially at high masses.

3 Seoul National University AGN Monitoring Project (SAMP)

The Seoul National University AGN Monitoring Project's (SAMP; PI Jonghak Woo, Seoul National University, Korea) goal is to monitor and obtain light lag times between the accretion disk and the BLR for AGNs with black hole masses more massive than most previous reverberation mapping campaigns. Such AGNs have not been studied in-depth due to the need for a long campaign baseline. Noticeable exceptions are the studies by e.g., Kaspi et al. (2017) and Lira et al. (2018) who report reverberation mapping of luminous quasars. Kaspi et al. (2017) measured the BLR size in C IV for three objects, Lira et al. (2018) present reverberation mapping results for 17 high-redshift high-luminosity quasars. [2,3] A monitoring campaign needs to be at least a year long with observations conducted every one to two weeks in order to detect the time delays for black holes as large as these, which can be on the order of months or more. The targets in our survey have black hole masses that range from 5.3 x 10^7 M_{Sun} to 5.9 x 10^9 M_{Sun}. Their redshift also varies from z = 0.127 to z = 0.343. Our targets are all in the northern sky and due to the physical limits of the Nickel telescope that we are using for observations, we cannot view objects with a Dec > 66°45' or with a zenith distance smaller than 6.9°. Our hour angle (HA)[1] constraints are from -4:20:00 (East) to +4:15:00 (West). Table 1 is a list of the AGNs we chose to study along with their coordinates.

This project is done in a collaboration between several groups, using two telescopes of Lick Observatory (in the mountains near San Jose, California). Nickel photometry (PI: Matt Malkan, UCLA, CoI: Cal Poly SAMP team and SAMP team in Korea) obtains continuum light-curves for around 40 bright AGNs using the CCD on the Nickel 40-inch telescope nearly once every 10 days. These same AGNs are observed spectroscopically using the Kast spectrograph on the 3m Shane telescope (PI Tommaso Treu, UCLA, CoI: SAMP team, Korea; SAMP team Cal Poly; Aaron Barth, Vivian U, Kyle Kabasares, and Dale Mudd, UC Irvine; Matt Malkan and Peter Williams, UCLA). Cal Poly joined SAMP near its beginning in January 2017, and the first students were checked out as official remote observers at Lick Observatory on January 27/28, 2017. Cal Poly's first night of observing was February 24, 2017, and our undergraduate team were in charge of photometric observations with the 1m Nickel telescope for 32 months. We have officially finished the program on September 5, 2019. We have had 73 observation nights total, with 42 successful nights of data. This thesis focuses only on the data collected from 2017 through the end of 2018. The data from the 2019 period is being reduced and analyzed for photometry purposes for this project by another Cal Poly undergraduate student, Nick Yee (in preparation).

---

[1]An hour angle is the angle between the meridian of the observer and the right ascension (RA) of the object of interest measured in hours and minutes. The meridian is a circle of constant longitude passing through the zenith of a given place on the earth's surface.

4   Observations

On a typical observing night, our observing team arrives an hour before sunset in order to set up the telescope as well as take the necessary calibration images. Once we are logged in remotely and have our GUIs (graphical user interfaces) set up on our three monitors, we first take 21 biases and expect the counts not to deviate from 1000 counts (a typical bias level) by more than 100. A bias is a zero second image at a controlled setting of 1000 counts in order to determine the underlying electron count level (due to a baseline current) at each pixel of the CCD without it being exposed to photons. All biases are later combined into a masterbias image (to reduce random noise) and subtracted out of the rest of the images. Right after sunset, we attempt to capture up to 7 sky flats in both B-filter and V-filter with counts ranging from 20,000 to 50,000. There is more red light towards the end of post-sunset, so we capture V-flats second. Once it is dark enough, we point the telescope using selected pointing stars from our coordinates file. These stars are chosen as pointing stars because they are bright enough to be used to point the telescope during our calibration time (during nautical twilight) before it is dark enough for our science images.

Once centered on a bright star near the zenith, we then focus the telescope by varying the position of the secondary mirror of the telescope. The positions are entered into a graphical user interface (GUI) and software calculates the best focus by comparing 7 to 9 short exposures of the same star with equal exposure times that are all in the same image but slightly offset from each other. Our GUI software tells us which focus gives us the focusing star with the smallest full-width half-max (FWHM) which means it is point-source like and focused. Finally, our observing night starts with standard star exposures of star fields of known magnitude. Once completed, we begin observations of our AGNs, typically with exposures of around 300 seconds (5 minutes) while our guider is monitoring a guiding star on an adjacent star field. Our guider GUI software monitors the x-y coordinates of a star we select and how it deviates from its initial position. It then autocorrects in real-time so that we stay locked onto our target without causing streaks on our exposures. Once the first exposure is read out, we compare it to the finding charts we have for all of our objects, like the examples shown on next page, to make sure we are centered on our target. All of our data for the night is continuously stored into the Lick Observatory data repository which is accessible online.

In the morning, we attempt to capture morning flats in both B and V filter again, starting with V in the morning as there is more red light. Once the sky is too bright and our flats are overexposed, we are able to close the mirror cover, park the telescope, and close the dome. We shut down all the software and log off from our remote connection before going home. Compiled in Table 2 are a list of all the SAMP observation nights for 2017. Table 3 is the similar list of all our SAMP observation nights for 2018.
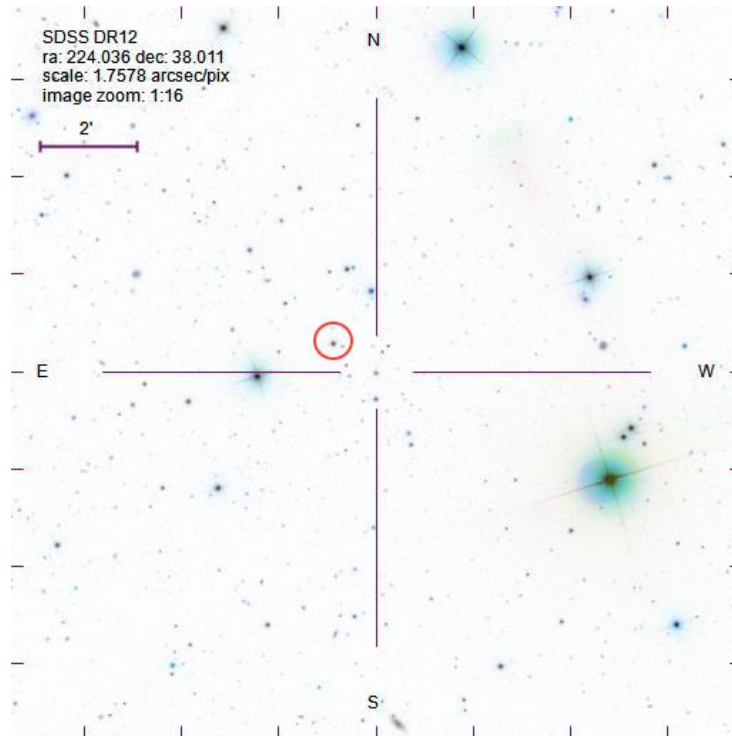
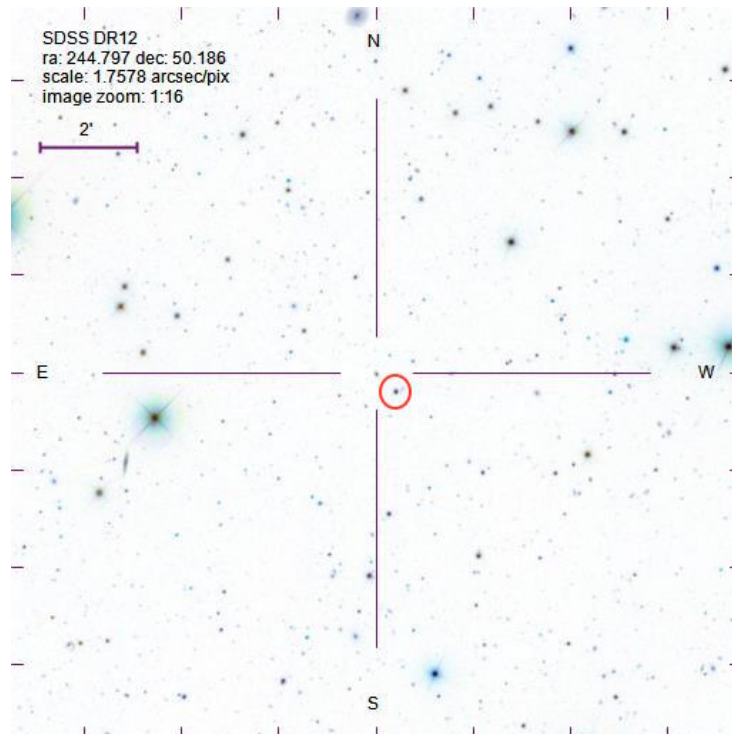Figure 6: An example of our finding chart for A38.

Figure 7: An example of our finding chart for A43.

SAMP AGN Objects with Coordinates				
Object Label	RA	Dec	z	B Magnitude
A01	1:01:31	42:29:36.0	0.190	16.7
A03	1:40:35	23:44:51.0	0.320	16.9
A04	2:27:40	44:10:00.0	0.175	18.4
A11	8:01:12	51:28:12.3	0.321	18.6
B01	8:03:09	53:00:04.8	0.287	18.5
B02	8:13:18	43:56:20.6	0.254	17.8
B04	8:48:53	28:24:11.8	0.198	18.3
B06	9:36:09	65:10:54.9	0.192	17.7
A14	9:39:40	37:57:05.8	0.231	18.0
A15	9:50:36	39:29:24.0	0.206	17.1
A18	10:59:36	66:57:58.0	0.340	17.7
B09	11:17:06	44:13:33.3	0.144	16.4
A23	11:20:07	42:35:51.4	0.226	17.8
A26	12:03:48	45:59:51.1	0.343	17.4
A29	12:17:52	33:34:47.3	0.178	17.5
A30	12:53:30	21:26:18.2	0.127	16.6
B18	13:23:50	65:41:48.2	0.168	15.9
A32	13:56:33	21:03:52.4	0.300	17.6
A36	14:15:36	48:35:43.6	0.275	17.8
B24	14:29:43	47:47:26.2	0.220	17
B26	14:42:07	35:26:23.0	0.079	15
B27	14:53:34.8	34:31:27.8	0.209	17.9
A38	14:56:09	38:00:38.6	0.283	17.3
A40	15:26:24	27:54:52.1	0.231	17.1
B31	15:35:39	56:44:06.5	0.207	17.8
A41	15:40:04	35:50:50.1	0.164	16.7
B32	15:42:35	57:41:41.9	0.245	18.4
A42	15:47:44	20:51:16.8	0.264	16.3
B35	16:14:13	26:04:16.3	0.131	16.4
A43	16:19:11	50:11:09.2	0.234	17.9
A47	19:35:21	53:14:12.1	0.248	16.1

Table 1: Above is a list of the final candidates of objects from our sample that we still observe along with astronomical information about each one. Object label pertains to how we identify the specific AGN along with its Right Ascension and Declination coordinates. The z column is the red shift of each AGN. The B magnitude (specifically around $\lambda = 440$ nm) is a logarithmic measurement of the apparent brightness of the object from Earth.

List of 2017 Cal Poly SAMP Team Observation Nights with 1m Nickel			
Date	Data Obtained	Reason	Observers
01/27/17	Training	− − − − −	V. Bennert, E. Donohue, **C. Spencer**, I. Stomberg
02/24/17	No	Humidity	V. Bennert, E. Donohue, **C. Spencer**, I. Stomberg
03/18/17	Yes	− − − − −	V. Bennert, E. Donohue, **C. Spencer**
04/04/17	No	Clouds	E. Donohue, E. Glad, **C. Spencer**
04/17/17	No	Rain	E. Donohue, **C. Spencer**, I. Stomberg
04/24/17	No	Fog	E. Donohue, I. Stomberg
05/02/17	Yes	− − − − −	E. Donohue, E. Glad, **C. Spencer**
05/15/17	Yes	− − − − −	E. Donohue, E. Glad, **C. Spencer**
06/01/17	Yes	− − − − −	E. Donohue, E. Glad, **C. Spencer**
06/26/17	Yes	− − − − −	E. Glad, **C. Spencer**, P. West
07/04/17	Yes	− − − − −	E. Glad, **C. Spencer**
07/13/17	Yes	− − − − −	E. Donohue, E. Glad, **C. Spencer**, P. West
07/23/17	Yes	− − − − −	E. Donohue, E. Glad, **C. Spencer**, P. West
08/01/17	Yes	− − − − −	E. Donohue, E. Glad, **C. Spencer**, P. West
08/04/17	Yes	− − − − −	E. Donohue, E. Glad
10/07/17	Yes	− − − − −	E. Glad, P. West, **C. Spencer**
11/12/17	Yes	− − − − −	E. Glad, P. West
11/13/17	No	Humidity	E. Glad, P. West, **C. Spencer**
12/15/17	No	Humidity	E. Donohue, P. West

Table 2: A table of observing nights from our campaign during 2017 listed with the date of the night the observations started on, whether data was successfully obtained that night, the reasons we were not able to observe if that was the case, and who the observers were for that given night.

List of 2018 Cal Poly SAMP Team Observation Nights with 1m Nickel			
Date	Data Obtained	Reason	Observers
01/21/18	No	Humidity	E. Glad, P. West
01/22/18	No	Humidity	T. Gibson, E. Glad, M. Ross, P. West
02/11/18	No	Ice	T. Gibson, E. Glad, M. Ross, P. West
02/24/18	No	Humidity	E. Glad, M. Ross, P. West
03/10/18	Yes	− − − − −	T. Gibson, M. Ross, P. West
03/23/18	No	Ice	T. Gibson, E. Glad, M. Ross, P. West
04/09/18	Yes	− − − − −	T. Gibson, E. Glad, M. Ross
04/22/18	Yes	− − − − −	**C. Spencer**, P. West
05/13/18	Yes	− − − − −	E. Glad, **C. Spencer**
05/15/18	No		M. Ross, **C. Spencer**
05/23/18	Yes	− − − − −	T. Gibson, E. Glad
05/25/18	No	Humidity	**C. Spencer**, P. West
06/04/18	Yes	− − − − −	T. Gibson, E. Glad, M. Ross, **C. Spencer**
06/18/18	Yes	− − − − −	M. Ross, **C. Spencer**
06/20/18	Yes	− − − − −	M. Ross, M. Salinas, **C. Spencer**
07/17/18	Yes	− − − − −	M. Salinas, **C. Spencer**
07/22/18	Yes	− − − − −	M. Salinas, **C. Spencer**
08/02/18	No	Particles	M. Salinas, **C. Spencer**
08/09/18	No	Particles	M. Ross, **C. Spencer**
08/21/18	Yes	− − − − −	M. Salinas, **C. Spencer**
09/01/18	No	Particles	M. Salinas, **C. Spencer**
09/10/18	Yes	− − − − −	M. Salinas, **C. Spencer**
10/04/18	No	Humidity	T. Gibson, E. Glad
10/17/18	Yes	− − − − −	M. Salinas, **C. Spencer**
11/06/18	Yes	− − − − −	T. Gibson, E. Glad, **C. Spencer**
11/14/18	No	Particles	E. Glad, M. Ross, M. Salinas
11/28/18	No	Rain	E. Glad, M. Ross, **C. Spencer**
12/05/18	No	Rain	T. Gibson, J. Hood, **C. Spencer**

Table 3: The same as in Table 2 but for 2018.

5   Data Reduction

From the 30 successful observing nights analyzed in this thesis, each night needs to be reduced using the calibration images from that day/night in the reduction process. Each successful night is uploaded into the Cal Poly Physics Dirac computer cluster for long-term storage and to run necessary programs used later on in order to reduce the data. The two main folders created for storage were "SAMP2017" and "SAMP2018" with their respective successful nights of data inside their own folders. The first step is to look through the images from each night and compile a series of 9 text files listing the image file names for every image type that are usable and document the examination process along with noted unusable images in a 10th text file. This is done with the help of a Python code and JupyterHub.

The criteria for usable bias images is an average of 1000 ± 100 counts. Cosmic rays could excite certain pixels yet are not much of a problem as they are eliminated by taking the average of 21 bias images in order to create a masterbias that is subtracted out of the rest of the images. For the flat field images taken shortly after sunset or shortly before sunrise, we want count levels that range between 25,000 - 55,000 counts. We exclude any sky flats with trails from planes or stars. The flat fields, both in B and V filter, are then able to be combined into masterflats and divided out of the rest of the images of their respective filter type.

Once the text files are made, they are uploaded into each respective night on the Dirac cluster. Using a program called PyRAF, supported by the Space Telescope Science Institute[2], I first input the bias text file in using a function called "zerocombine" in order to create a masterbias (see Appendix Figure I). In this step, the Nickel CCD's read noise of 10.7 and gain of 1.8 need to be entered into the lower half of the GUI. Next, I input the text file for the rest of the images to be reduced and an output file to convert all the bias reduced images to include a "_Z" at the end of the file name (see Appendix Figure II & III). I also check "yes" for using the zerocor program and identifying the bias to use as "masterbias". A function called "flatcombine" is used to create masterflats for both the B and V filter flats from an input list of flats in their respective filters (Appendix Figure IV and Figure V). The read noise and gain also are entered in this GUI. Finally, I input a list of either B or V objects to have the B or V masterflat divided out of with an output list included the same images with a "_ZF" included at the end of the file name (Appendix Figure VI). In this step, I check "no" on the zerocor function and "yes" on the flatcor function. It is also important to identify the masterflat to be divided out in the lower GUI section.

---

6 Data Analysis

Once the images are reduced, I write a source code file which extracts the respective AGNs from the folders of the nights they were observed to new folders as well as renaming them in the process with a file name that includes the AGN title, the date observed, and which exposure in the sequence it was. The last label is due to the fact that most of these AGNs have two or three exposures taken of the same object in the same location directly back to back. These are transferred into a folder called "1_AGN_Sort" as they have been sorted by their AGN identification label. Next, I check for three things in deciding whether the various images of an AGN are able to be combined: confirming which nights these AGNs were observed more than once, seeing which ones were usable, and finally making sure the field-of-view (FOV) does not change at all so that the positions of the stars and AGN match between exposures. They are then copied to a folder called "2_AGN_Combine" and combined together using the command "imcombine" in PyRAF. Both the combined images and the single exposure images of our AGNs are copied to a final folder called "3_AGN_Phot".

Now that all the images are ready for photometry, I first go through and edit the parameters of the PyRAF windows in Appendix 10.2 Figure VII through Figures X with the ideal setting based on the FWHM of the AGNs, sky background counts, etc. In the datapars window, sigma, the min and max of the data, read noise, and gain are all required to be entered (Appendix Figure VII). Next, select "centroid" as the centering algorithm with a specific cbox (Appendix Figure VIII). In the photpars GUI, input the radii of the aperture which can be found from creating a curve of growth with multiple radii levels (Appendix Figure IX). Input an annulus and dannulus in the fitskypars GUI so the software knows how to analyze the objects with respect to the sky around them (Appendix Figure X). Then, I run daofind in order to create .coo files for each image in the list that will be used to find the magnitudes of the objects at the given coordinates in the .coo file (Appendix Figure XI). The original coordinates are discarded and the correct ones are found using the command "imexam" and the cursor in order to find the x-y coordinates of the AGN and comparison stars for each image used in "3_AGN_Phot". Finally, the edited .coo file is used to run the photometry process and output a .mag file for each image in the folder with individual magnitudes for each object noted in each of the .coo files (Appendix Figure XII). The results are extracted from all of the .mag files into one text file that was analyzed first with Excel and then with MATLAB. Examples of an image of our analyzed objects with the AGN and their comparison stars identified are shown as Figures 8 and 9 on the next page. The light-curves generated from the photometry are shown in the Results section as Figure 10 and Figure 11.
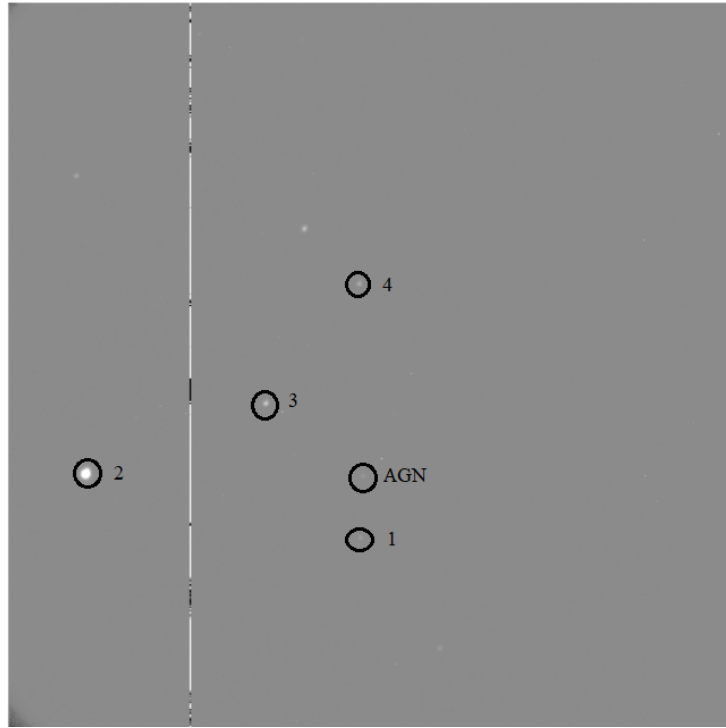
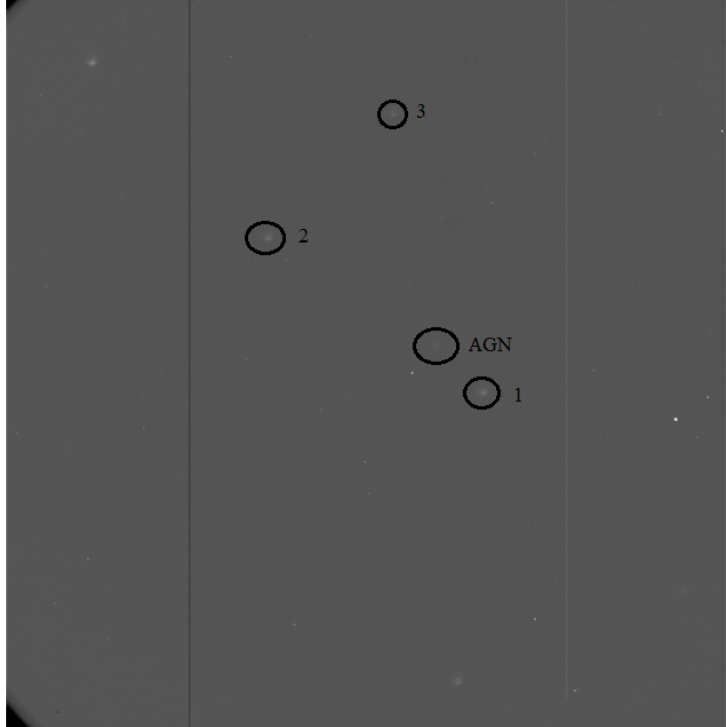Figure 8: An exposure of AGN object A38 with AGN and comparison stars identified.

Figure 9: Same as Figure 8, but for AGN object A43.

7   Results and Discussion

By following the PyRAF procedures and customizing the settings to the characteristics of our field-of-view and AGN objects, a list of magnitudes was created by PyRAF for our AGNs and comparison stars for each night they were observed. I averaged the comparison stars and compared them against each other to initially confirm that they are all non-variable in flux. Then, I compared that light curve of non-variable comparison stars to the changing flux of the AGN in order to create the two figures below. Figure 10 shows the differential light-curve for AGN object A38, and Figure 11 shows the same for A43 (see Table 1 for more details). A38 shows a magnitude difference of at least 0.443 ± 0.05 mag by going off of the nights we are able to extrapolate from. A43 shows a magnitude difference of at least 0.315 ± 0.05 mag by the same estimation.

As mentioned in the introduction, our imaging data from the 1m Nickel telescope can be combined with spectroscopic data from the BLR of these AGNs in order to perform reverberation mapping. By finding the time difference between the peak flux of the optical continuum near the accretion disk that we observe with the 1m Nickel telescope and the peaks in emission flux, we are able to calculate the radius of the BLR. We can calculate the velocity of the gas in the AGN from Doppler broadening of the Hβ line in the spectra of the BLR obtained with the 3m Shane telescope. This ultimately can be used to estimate the mass of the black hole. This is beyond the scope of this thesis, but is work in progress by the SAMP team.
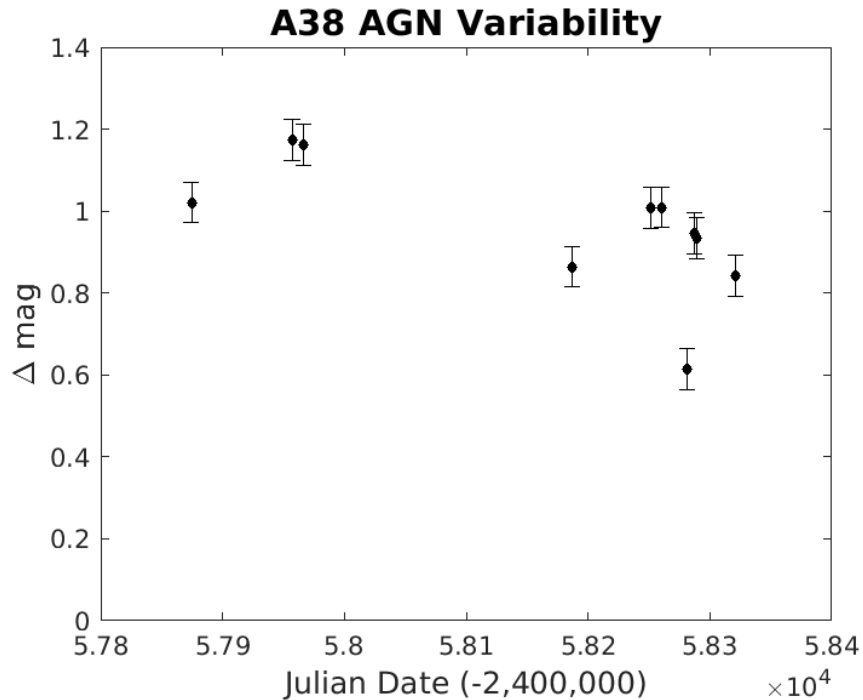

Figure 10: Differential light-curve for AGN object A38 [z = 0.283].
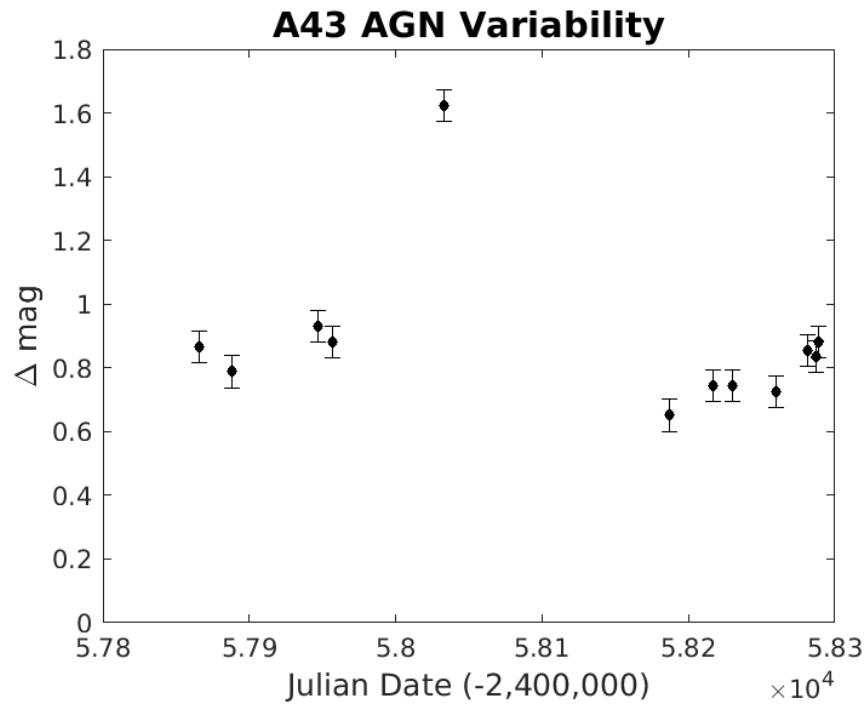
Figure 11: Same as Figure 8, but for AGN object A43 [z = 0.234].

8   Summary

In conclusion, the results in this paper are a small contribution towards a joint collaboration called the Seoul AGN Monitoring Project (SAMP) between Cal Poly San Luis Obispo, UCLA, UCI, and Seoul National University (SNU). Our team of undergraduate students from Cal Poly remotely logged into the 1m Nickel telescope located at Lick Observatory an hour east of San Jose, CA from our remote observing room in the Baker Science building on the Cal Poly campus. The team collected optical images from an AGN sample of $\approx$80 AGNs for over two and a half years. After several months of observations, we narrowed down our survey sample to 31 candidates that exhibit significant optical continuum variability. The long length of this campaign was necessary as the lag times of these AGNs are larger than previous campaigns since the black holes inside are more massive, and the accretion disks more luminous and therefore create a greater distance between the accretion disk and the broad line region (BLR). Ultimately, the light-curves generated for this paper can be combined with spectroscopic exposures taken of the BLR of the same objects in order to estimate the masses of the black holes inside via reverberation mapping.

Using data reduction techniques and the software program PyRAF, the data was reduced using the calibration images. Then, we performed differential photometry by comparing the optical variability of our AGN objects over time against comparison stars in the same field-of-view. As a result, the previously shown light-curves, Figure 10 and Figure 11, were created from this process and seem to show that these AGNs do indeed exhibit optical continuum variability over large time scales. A38 shows a magnitude difference of at least 0.443 ± 0.05 mag, and A43 with a magnitude difference of at least 0.315 ± 0.05 mag. The continuation of creating light curves for the remaining objects is work that will be continued by the SAMP team.

9   Acknowledgements

10   Appendix

10.1   Data Reduction
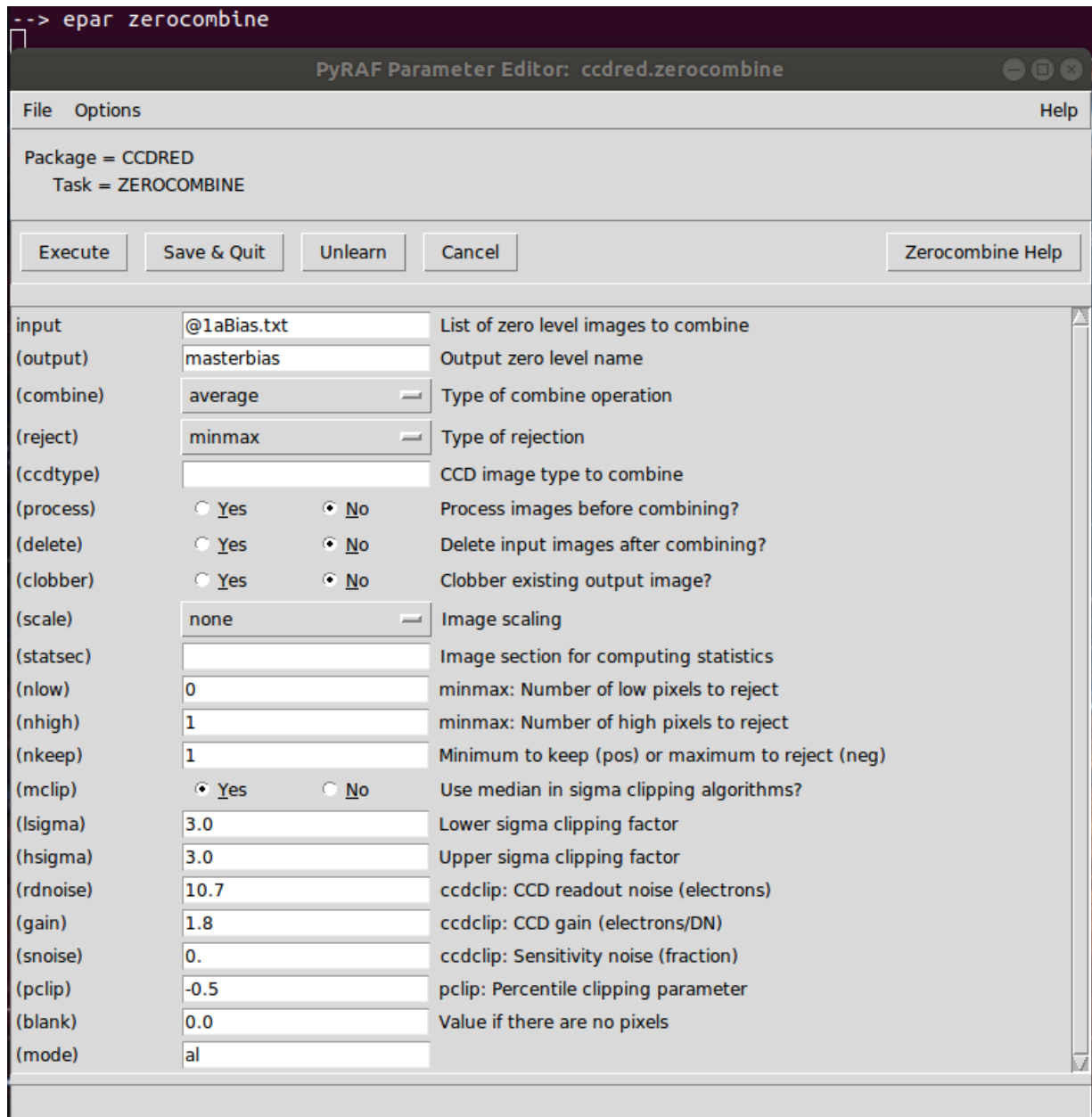
Figure I: A screenshot of the PyRAF epar window for making a masterflat. In the input line, enter a list of acceptable biases and label the output "masterbias". Verify that it is combining using the "average" and rejecting using "minmax", but those are typically default settings. Finally, the read noise and gain of the CCD of the Nickel telescope need to be entered.
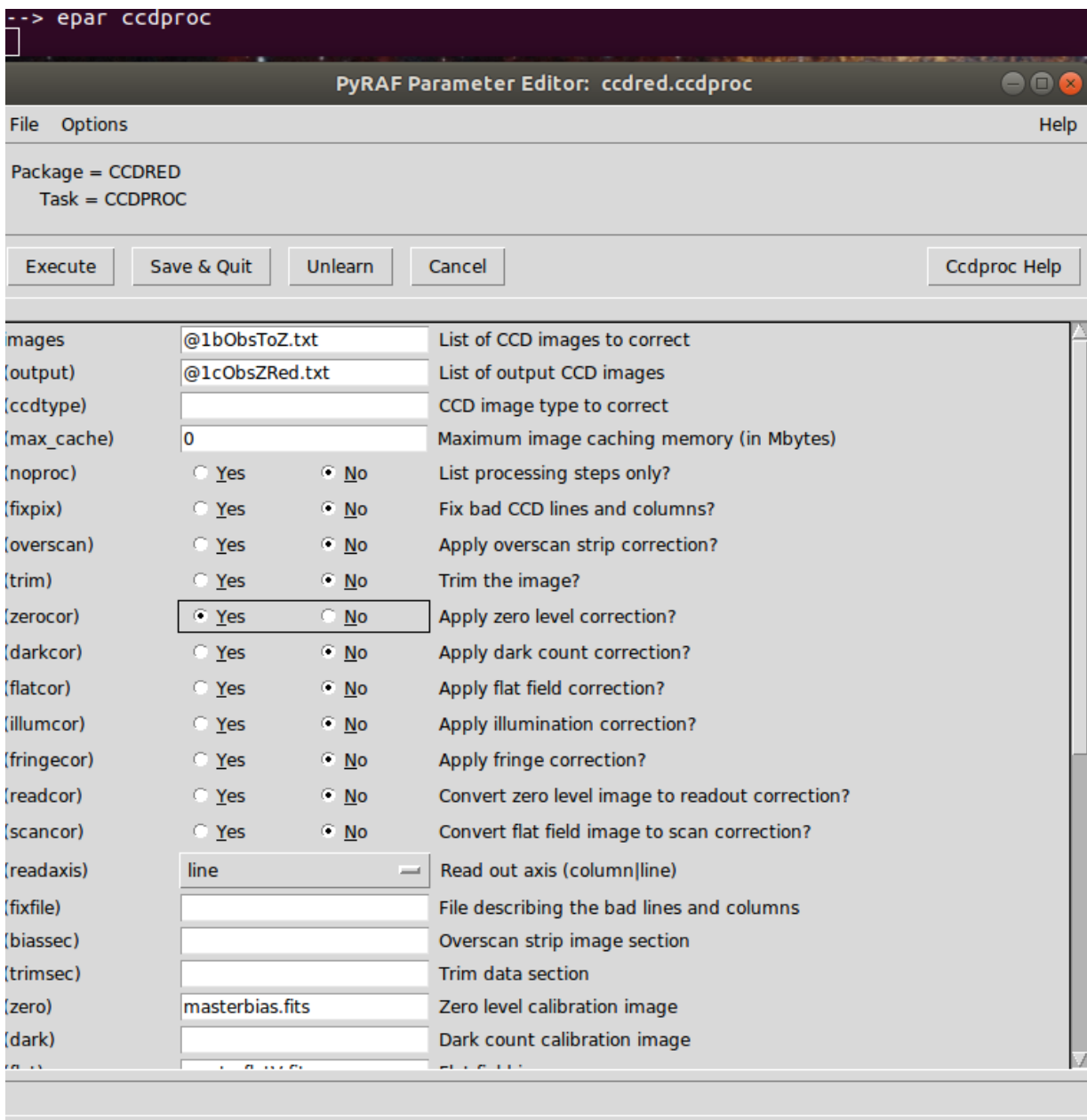
Figure II: A screenshot of PyRAF epar window for subtracting the masterbias out from the other exposures. The top entry is for inputting a list of CCD images that will have the masterbias subtracted from them. The output is what the names of these images will be after they are reduced. I added a "_Z" at the end of each image in order to signify successfully "zero reducing" them. The only other critical steps is checking "yes" for the zerocor function and identifying the name of your masterbias.

```
--> epar ccdproc
```

(dark)		Dark count calibration image
(flat)	masterflatB.fits	Flat field images
(illum)		Illumination correction images
(fringe)		Fringe correction images
(minreplace)	1.0	Minimum flat field value
(scantype)	shortscan	Scan type (shortscan|longscan)
(nscan)	1	Number of short scan lines
(interactive)	○ Yes ● No	Fit overscan interactively?
(function)	legendre	Fitting function
(order)	1	Number of polynomial terms or spline pieces
(sample)	*	Sample points to fit
(naverage)	1	Number of sample points to combine
(niterate)	1	Number of rejection iterations
(low_reject)	3.0	Low sigma rejection factor
(high_reject)	3.0	High sigma rejection factor
(grow)	0.0	Rejection growing radius
(mode)	al	

Figure III: An extension of Figure II's lower GUI area. While this region does not need to be altered in this step, this ccdproc function, which stands for CCD Procedure, is also used to divide the masterflats out of images as well. In the "flat" entry, my masterflat for the B filter is identified for the program. This needs to be changed when dividing out B and V respectively.

```
--> epar flatcombine
```

PyRAF Parameter Editor: ccdred.flatcombine

File   Options   Help

Package = CCDRED
    Task = FLATCOMBINE

| Execute | Save & Quit | Unlearn | Cancel | | Flatcombine Help |

input	@2aBFlats.txt	List of flat field images to combine
(output)	masterflatB	Output flat field root name
(combine)	median	Type of combine operation
(reject)	avsigclip	Type of rejection
(ccdtype)		CCD image type to combine
(process)	○ Yes ⊙ No	Process images before combining?
(subsets)	○ Yes ⊙ No	Combine images by subset parameter?
(delete)	○ Yes ⊙ No	Delete input images after combining?
(clobber)	○ Yes ⊙ No	Clobber existing output image?
(scale)	median	Image scaling
(statsec)	[317:829,236:804]	Image section for computing statistics
(nlow)	1	minmax: Number of low pixels to reject
(nhigh)	1	minmax: Number of high pixels to reject
(nkeep)	1	Minimum to keep (pos) or maximum to reject (neg)
(mclip)	⊙ Yes ○ No	Use median in sigma clipping algorithms?
(lsigma)	3.0	Lower sigma clipping factor
(hsigma)	3.0	Upper sigma clipping factor
(rdnoise)	10.7	ccdclip: CCD readout noise (electrons)
(gain)	1.8	ccdclip: CCD gain (electrons/DN)
(snoise)	0.	ccdclip: Sensitivity noise (fraction)
(pclip)	-0.5	pclip: Percentile clipping parameter
(blank)	1.0	Value if there are no pixels
(mode)	al	

Figure IV: A screenshot of the PyRAF epar window for making a masterflat. The step currently shown is for the V filter, but is repeated for B filter. Input a list of flats for the filter that you are creating a masterflat for and output a label for the specific masterflat. The statsec region is the region from the flats that you are choosing to create masterflats from. The ideal flat field region can vary between CCDs, but you should also use your own discretion when selecting a region. Finally, the read noise and gain need to be entered in the lower GUI as well.

```
--> epar ccdproc
```

PyRAF Parameter Editor: ccdred.ccdproc

File   Options   Help

Package = CCDRED
   Task = CCDPROC

| Execute | Save & Quit | Unlearn | Cancel | | Ccdproc Help |

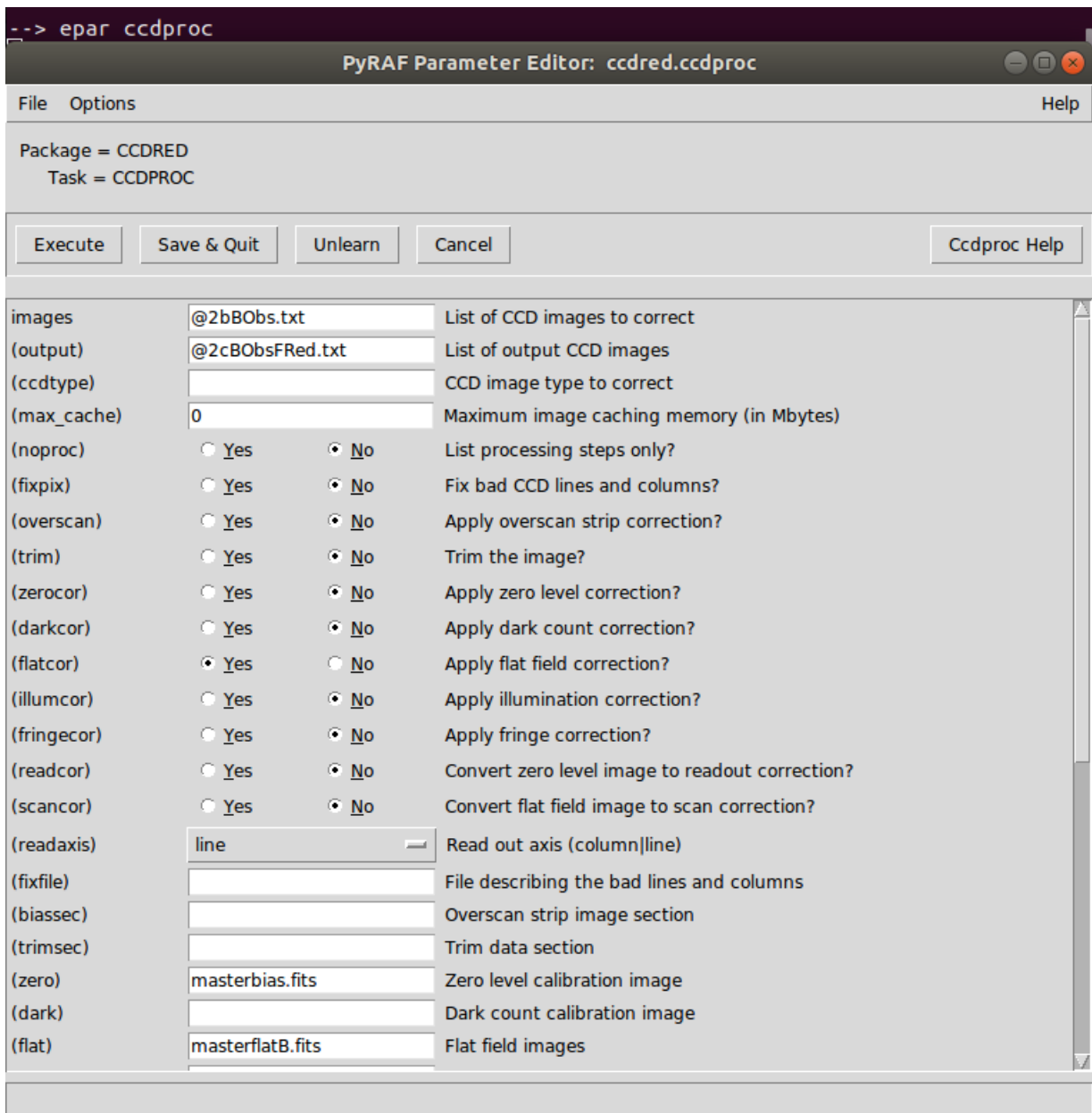| images | @2bBObs.txt | List of CCD images to correct |
(output)	@2cBObsFRed.txt	List of output CCD images
(ccdtype)		CCD image type to correct
(max_cache)	0	Maximum image caching memory (in Mbytes)
(noproc)	○ Yes ● No	List processing steps only?
(fixpix)	○ Yes ● No	Fix bad CCD lines and columns?
(overscan)	○ Yes ● No	Apply overscan strip correction?
(trim)	○ Yes ● No	Trim the image?
(zerocor)	○ Yes ● No	Apply zero level correction?
(darkcor)	○ Yes ● No	Apply dark count correction?
(flatcor)	● Yes ○ No	Apply flat field correction?
(illumcor)	○ Yes ● No	Apply illumination correction?
(fringecor)	○ Yes ● No	Apply fringe correction?
(readcor)	○ Yes ● No	Convert zero level image to readout correction?
(scancor)	○ Yes ● No	Convert flat field image to scan correction?
(readaxis)	line	Read out axis (column|line)
(fixfile)		File describing the bad lines and columns
(biassec)		Overscan strip image section
(trimsec)		Trim data section
(zero)	masterbias.fits	Zero level calibration image
(dark)		Dark count calibration image
(flat)	masterflatB.fits	Flat field images

Figure V: A screenshot of the PyRAF epar window for dividing out the masterflat for B filter from the science images. As stated previously in the appendix, this is the same GUI used to subtract masterbiases from your images. Check "no" for zerocor and "yes" for flatcor in order to switch over to flat correcting. The only entries to mind between filters are the input, output, and flat at the bottom of the GUI to identify the masterflat for a specific filter.
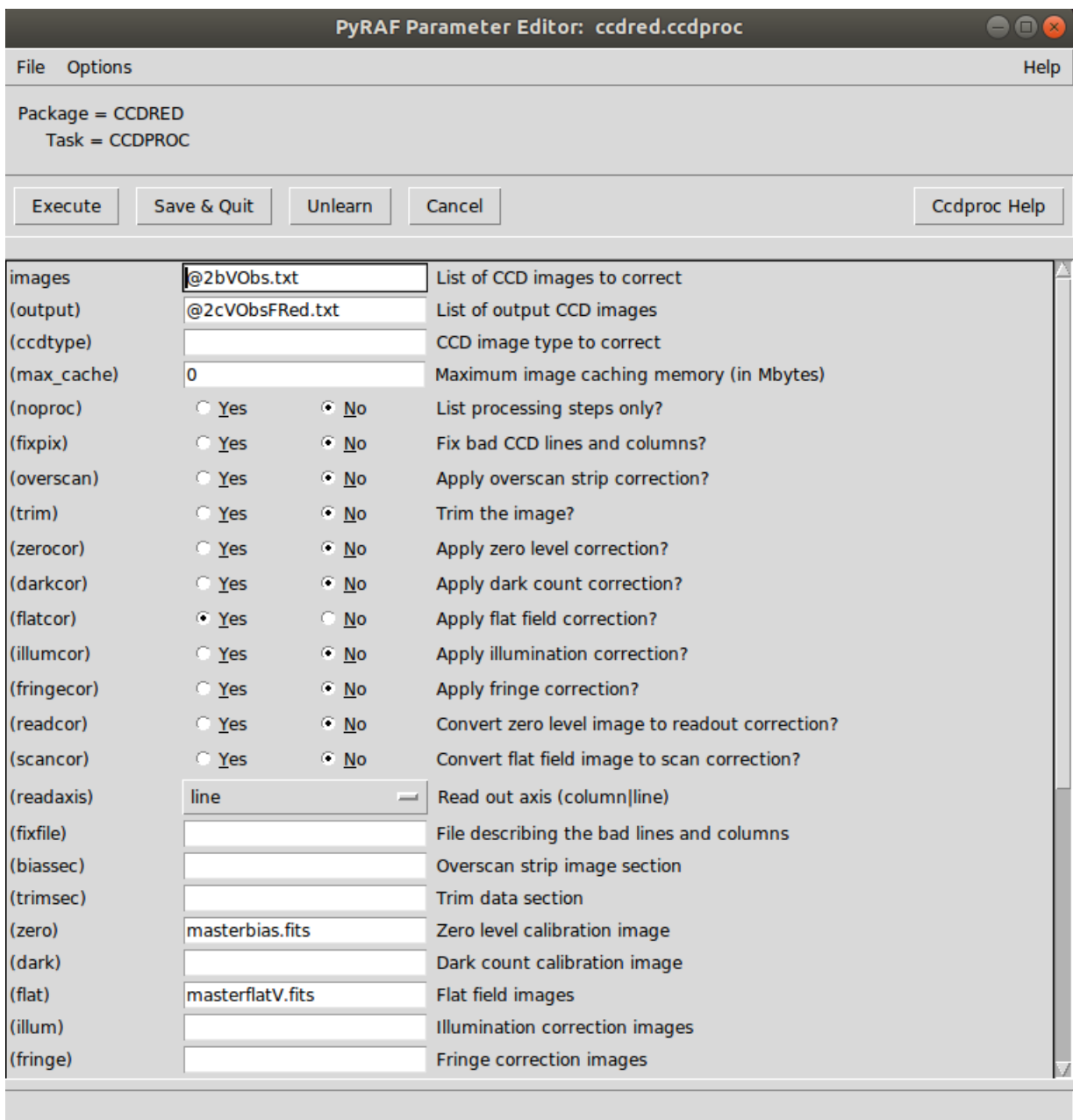
Figure VI: A screenshot of the PyRAF epar window for dividing out the masterflat for V filter from the science images. This is the last step of data reduction. Now each exposure should have "_ZF" at the end of their image name.
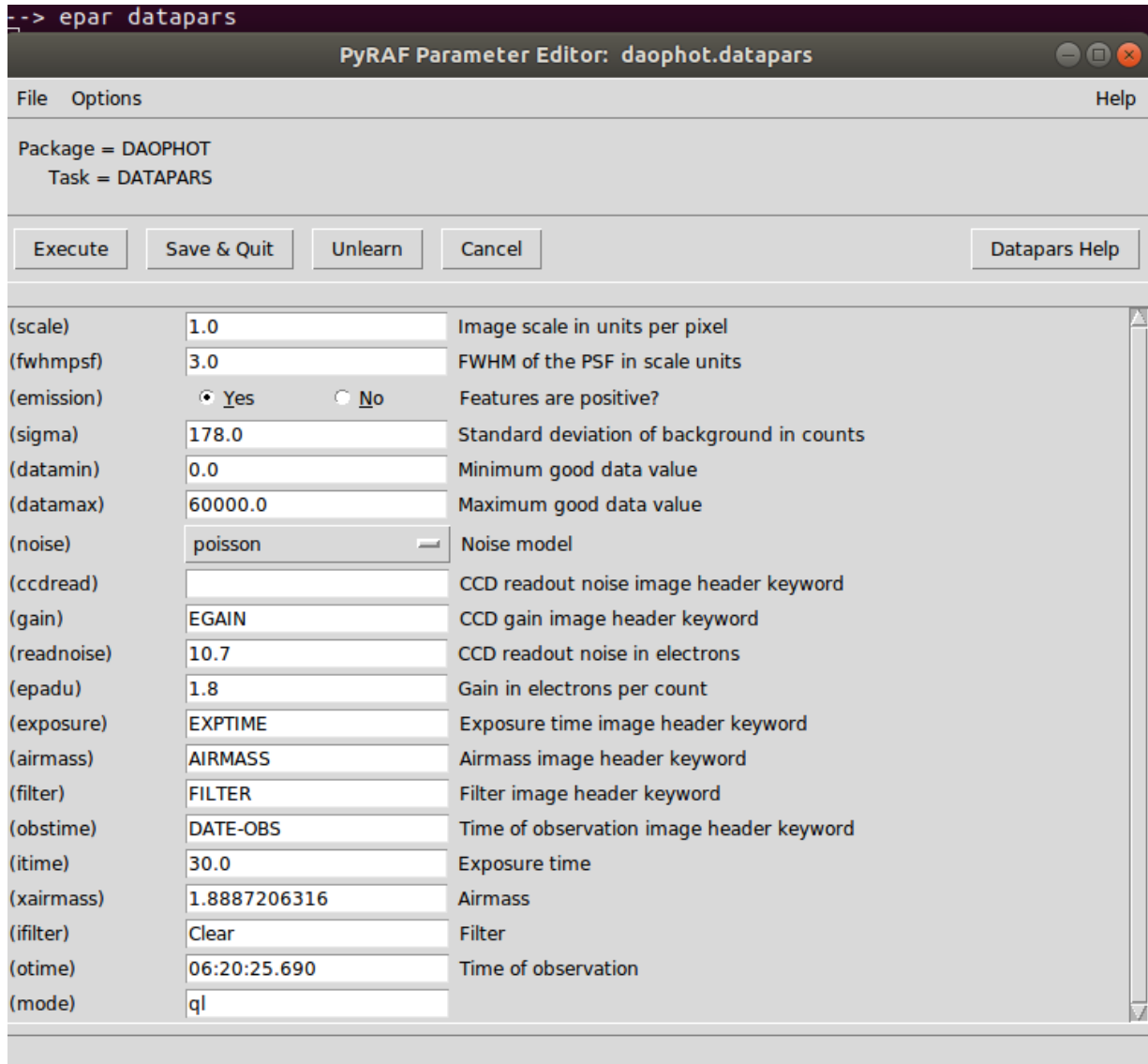
10.2 Data Analysis

Figure VII: A screenshot of the PyRAF epar window for key information about the data set such as CCD settings. The five entries to edit in this GUI is: sigma, data min, data max, read noise, and gain. Sigma, also known as your standard deviation, can be determined by examining the image with PyRAF tools. Data min and max range from 0 to 60,000 counts, as that is the range of our CCD.
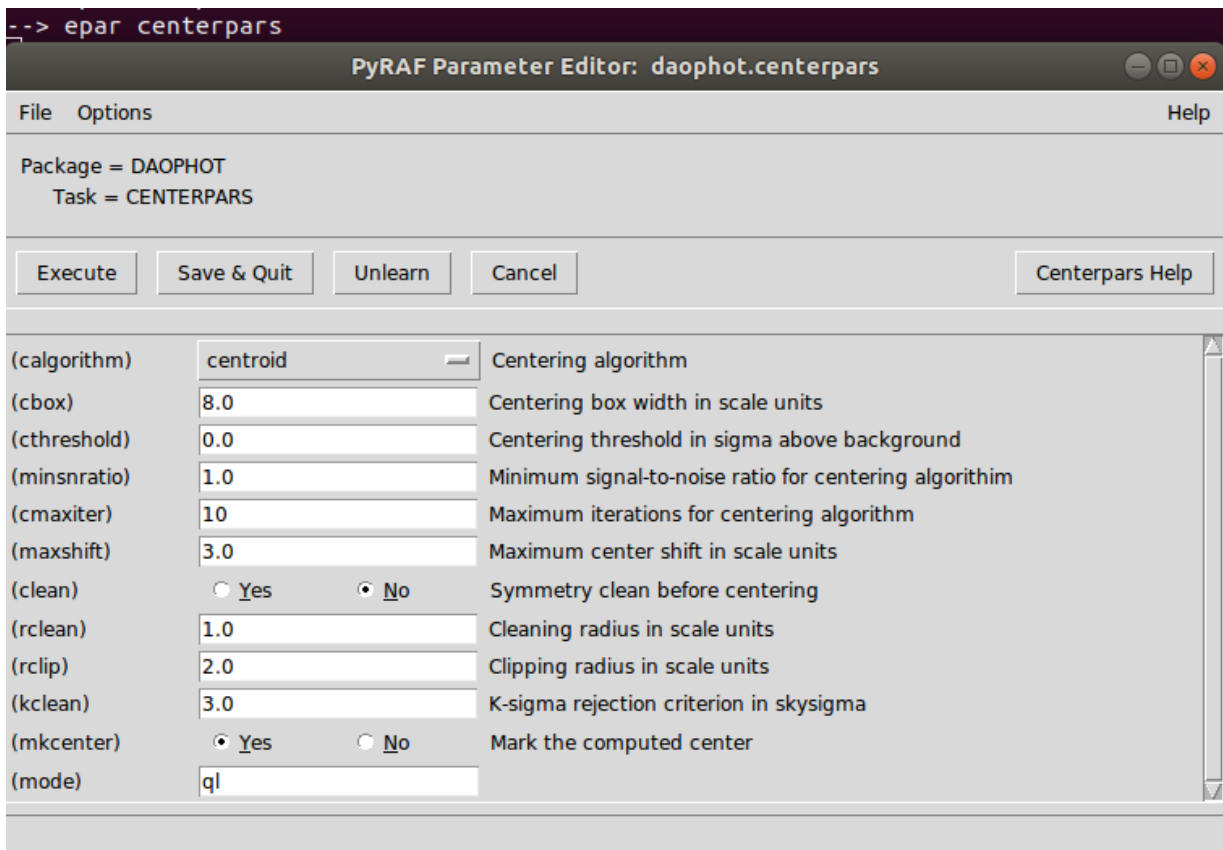
Figure VIII: A screenshot of the PyRAF epar window for editing the parameters of the photometry program. In this analysis, centroid was the centering algorithm used with a cbox of 8 scale units. Ideally, the cbox should be set to double the FWHM of your AGN/stars.
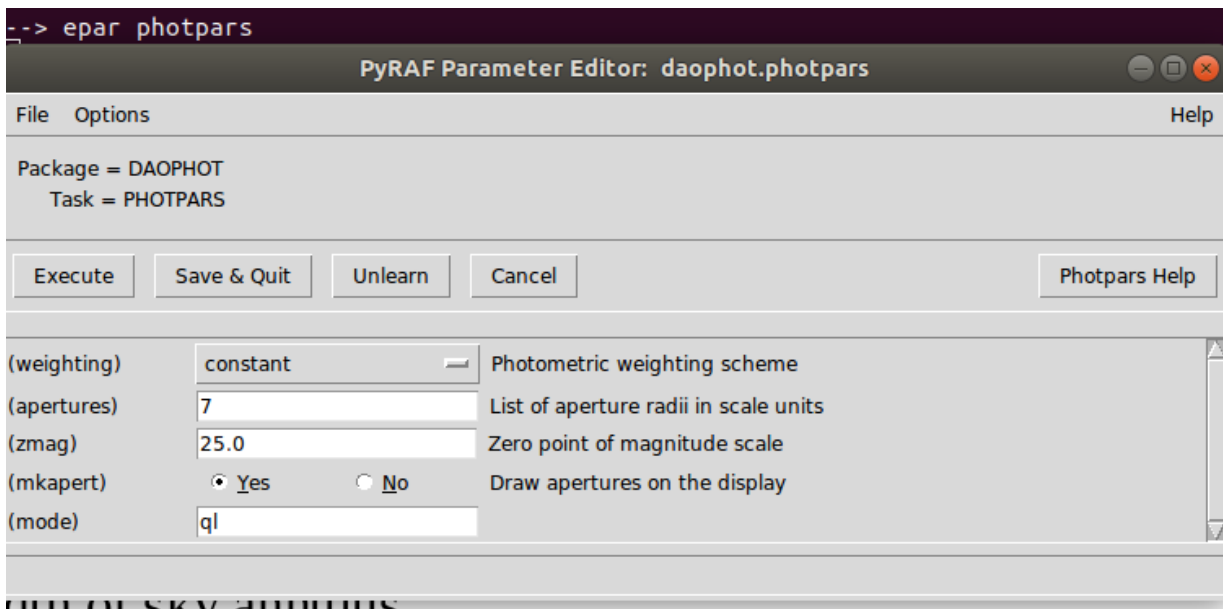
Figure IX: A screenshot of the PyRAF epar window for editing the photometry parameters. The only thing changed in this GUI is the aperture radii in scale units. The aperture radii is determined by creating a curve of growth and comparing the radius aperture compared to the signal coming from the object over the noise.
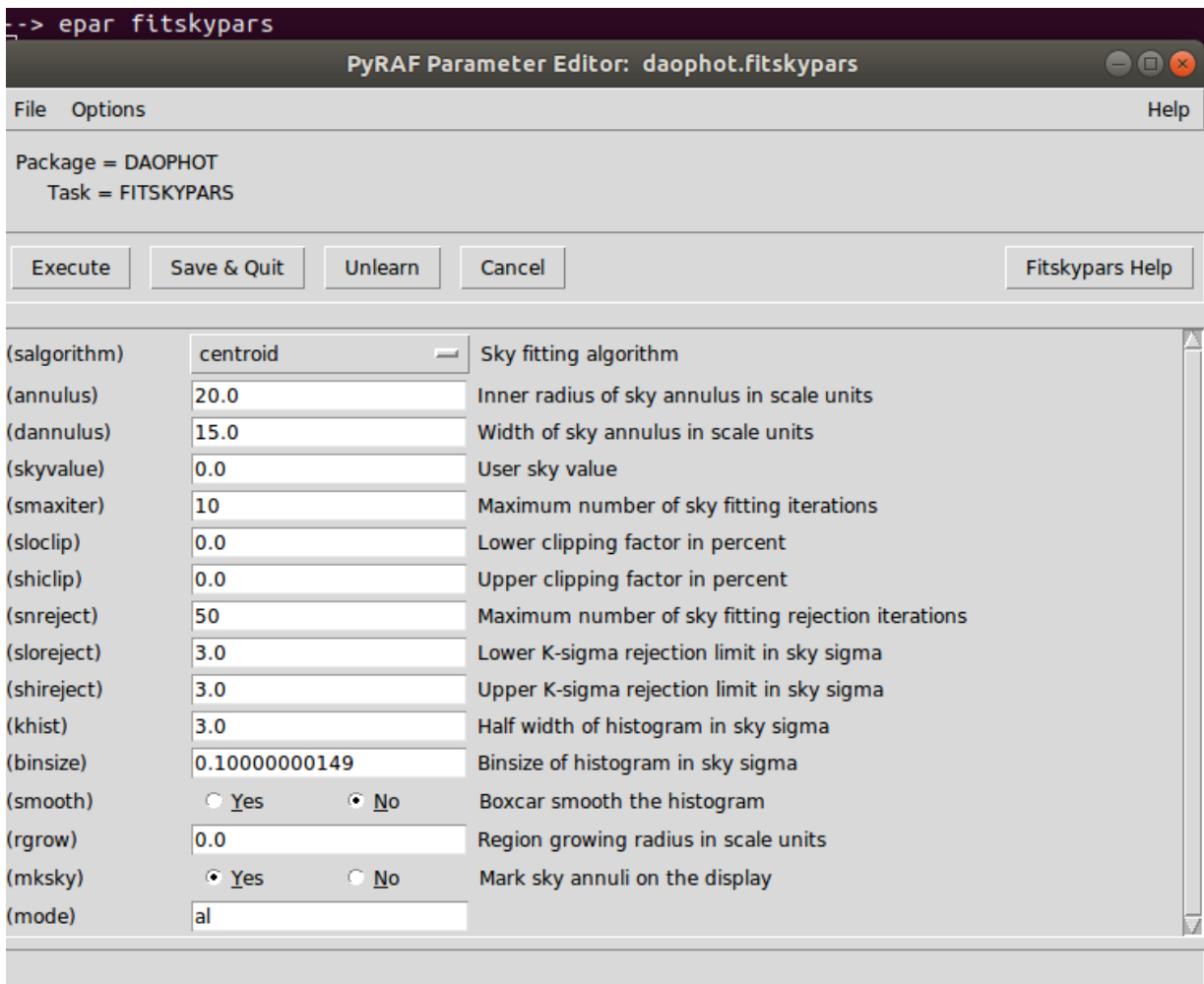
Figure X: A screenshot of the PyRAF epar window for editing the sky parameters of the photometry software such as the radius of the sky annulus. The annulus and dannulus are both inputs that you need to alter based on reasoning from the data. The dannulus should be 5 scale units smaller than the annulus.
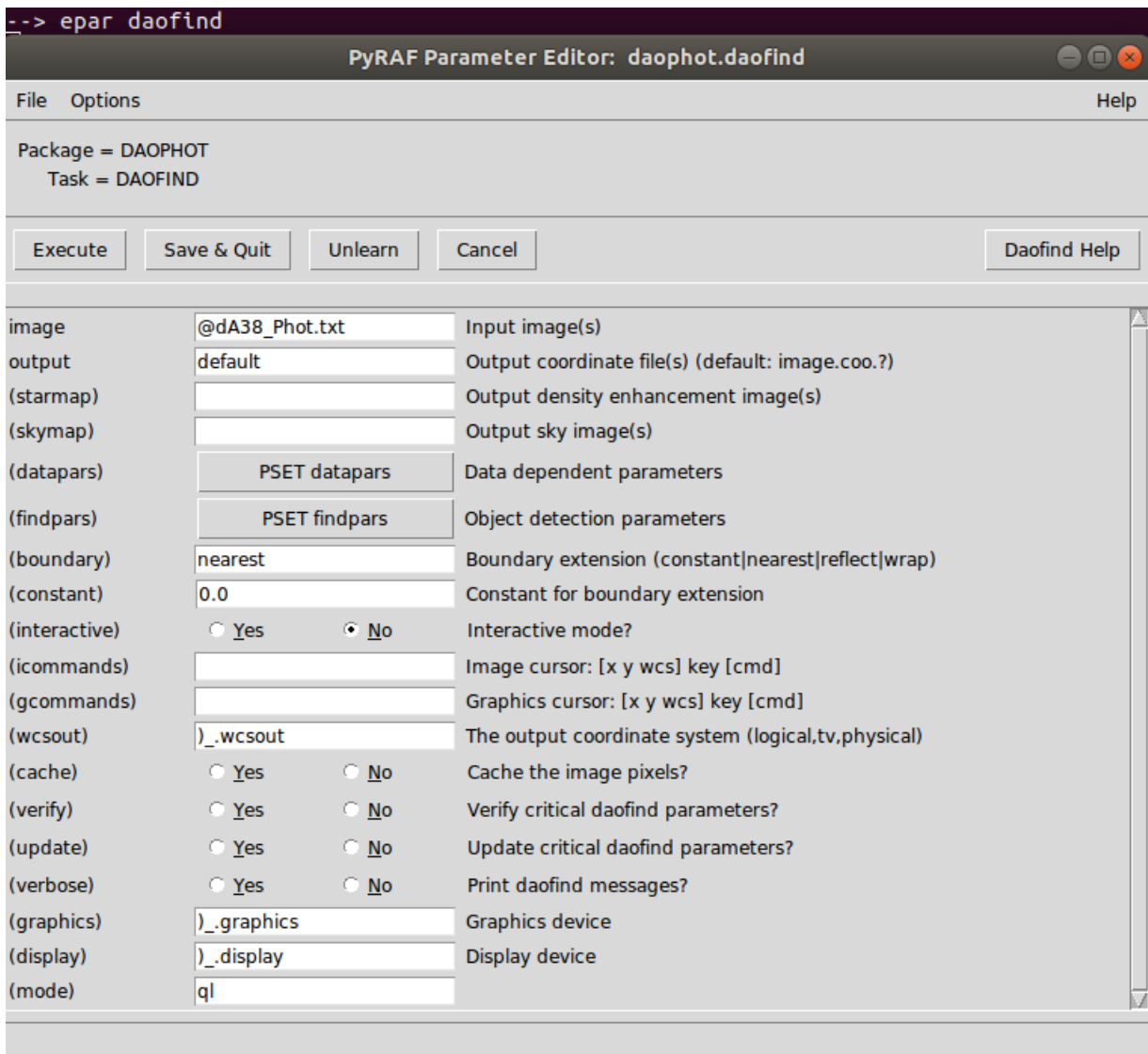
Figure XI: A screenshot of the PyRAF epar window for running daofind which creates a .coo file which lists the coordinates of the found stars based on your criteria. In this study, we did not use the coordinates output by the program, but instead altered the .coo files and emulated their structure but manually input the coordinates of our comparison stars and AGN object by hand. The important step in this GUI is to input the list of images for coordinate files to be created for.

```
--> epar findpars
```

File   Options   Help

Package = DAOPHOT
    Task = PHOT

[Execute]   [Save & Quit]   [Unlearn]   [Cancel]   [Phot Help]

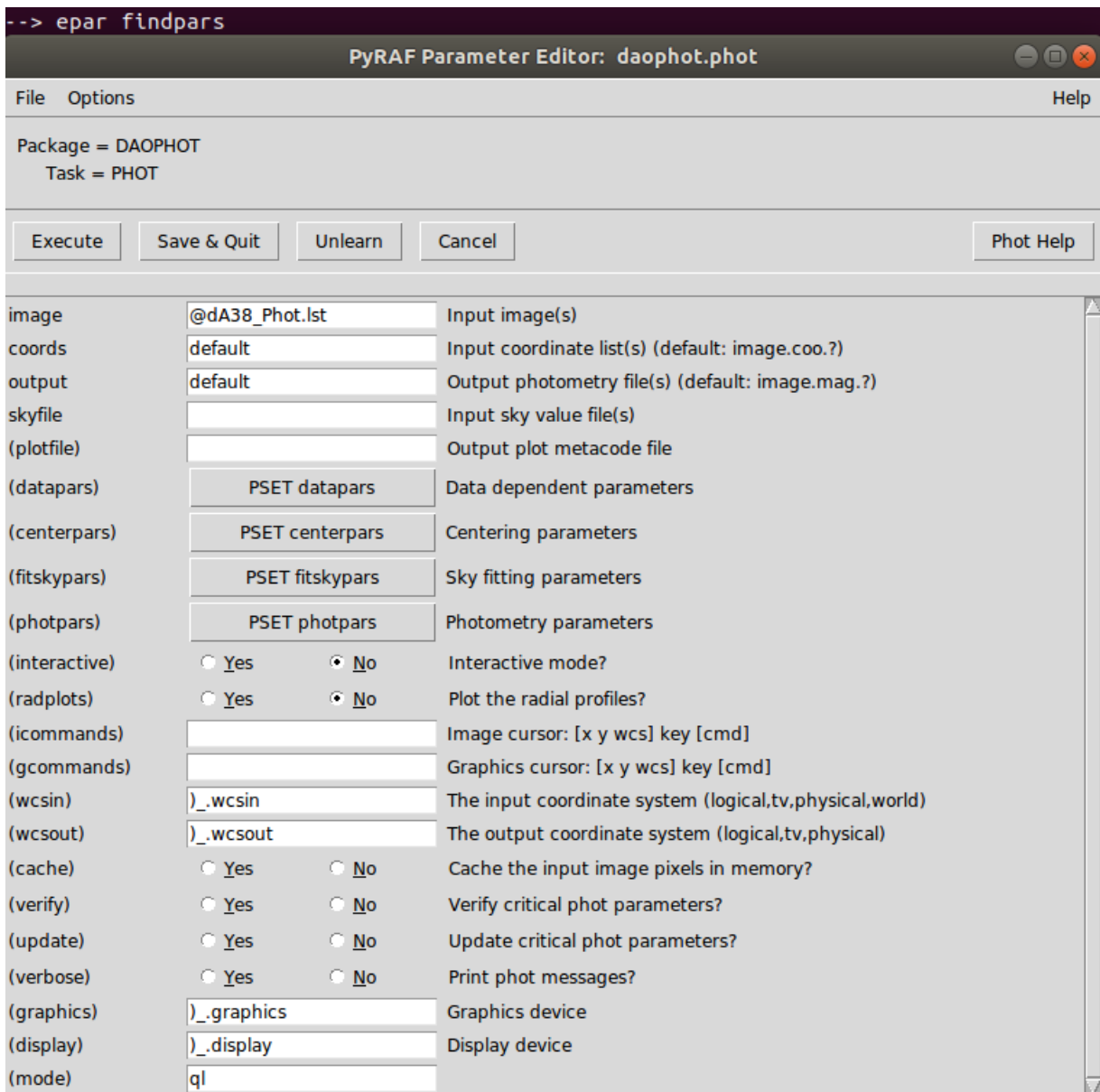| image | @dA38_Phot.lst | Input image(s) |
coords	default	Input coordinate list(s) (default: image.coo.?)
output	default	Output photometry file(s) (default: image.mag.?)
skyfile		Input sky value file(s)
(plotfile)		Output plot metacode file
(datapars)	PSET datapars	Data dependent parameters
(centerpars)	PSET centerpars	Centering parameters
(fitskypars)	PSET fitskypars	Sky fitting parameters
(photpars)	PSET photpars	Photometry parameters
(interactive)	○ Yes ◉ No	Interactive mode?
(radplots)	○ Yes ◉ No	Plot the radial profiles?
(icommands)		Image cursor: [x y wcs] key [cmd]
(gcommands)		Graphics cursor: [x y wcs] key [cmd]
(wcsin)	)_.wcsin	The input coordinate system (logical,tv,physical,world)
(wcsout)	)_.wcsout	The output coordinate system (logical,tv,physical)
(cache)	○ Yes ○ No	Cache the input image pixels in memory?
(verify)	○ Yes ○ No	Verify critical phot parameters?
(update)	○ Yes ○ No	Update critical phot parameters?
(verbose)	○ Yes ○ No	Print phot messages?
(graphics)	)_.graphics	Graphics device
(display)	)_.display	Display device
(mode)	ql	

Figure XII: A screenshot of the PyRAF epar window for making the program perform photometry on the image list and output a .mag file. With the same images with .coo files created, input a list to analyze with photometry. Leave coords and output as "default".

11   References

[1] Bentz et al. 2006, The Astrophysical Journal, 651, 775

[2] Kaspi et al. 2017, "Reverberation Mapping of High-Luminosity Quasaras", Frontiers Astronomy Space Science.

[3] Lira, P, Botti, I, Kaspi, S, Netzer, H, 2018, "Reverberation Mapping of High-Z, High-Luminosity Quasars", Frontiers Astronomy Space Science.

[4] Morgan, Siobahn. Distant and Weird Galaxies. 2002.

   http://www.uni.edu/morgans/astro/course/Notes/section3/new13.html

[5] Peterson, B.M. *An Introduction to Active Galactic Nuclei.* Cambridge University Press, Cambridge, Massachusetts, 1997.

[6] Urry & Padovani 1995, Publications of the Astronomical Society of the Pacific, 107, 803